

1 **Measurement Report: Rapid changes of chemical characteristics and health risks for high**
2 **time-resolved trace elements in PM_{2.5} in a typical industrial city in response to stringent**
3 **clean air actions**

4 Rui Li^{a*}, Yining Gao^a, Yubao Chen^a, Meng Peng^{b,c*}, Weidong Zhao^{c*}, Gehui Wang^a, Jiming Hao^b

5 ^a Key Laboratory of Geographic Information Science of the Ministry of Education, School of
6 Geographic Sciences, East China Normal University, Shanghai, 200241, P.R. China

7 ^b State Key Joint Laboratory of Environment Simulation and Pollution Control, School of
8 Environment, Tsinghua University, Beijing, 100084, P.R. China

9 ^c Institute of ~~energy~~ Energy conservation and ~~environmental~~ Environmental protection Protection,
10 China Electronic Information Industry Development Research Institute, Beijing, 100084, P.R. China

11 *** Correspondence to:**

12 Prof. Li (rli@geo.ecnu.edu.cn), Dr. Peng (mvponesky@163.com), and Prof. Zhao

13 (zhaoweidong@ccidthinktank.com)

14 **Abstract**

15 Atmospheric trace metals entail significant damages in human health and ecosystem safety, and
16 thus a series of clean air actions have been implemented to decrease the ambient element
17 concentrations. Unfortunately, the impact of these emission control measures on element
18 concentrations in fine particles ~~remained~~ ~~remains~~ poorly understood. In our study, the random forest
19 (RF) model was applied to distinguish the effects of emission and meteorology to trace elements in
20 PM_{2.5} in a typical industrial city named Tangshan based on a three-year (2017-2020) hourly field
21 observation. The result suggested that the clean air actions have facilitated the dramatic decreases
22 of the deweathered concentrations of Ga, Co, Pb, Zn, and As by 72%, 67%, 62%, 59%, and 54%,
23 respectively. It is attributable to the strict implementation of “coal to gas” strategies and
24 optimization of industrial structure and layout. However, the deweathered levels of Ca (8.3%), Cr
25 (18.5%), and Fe (23%) only displayed minor decreases, indicating that the emission control
26 measures for ferrous metal smelting and vehicle emission were not very effective. The positive
27 matrix factorization (PMF) results suggested that the contribution ratios of biomass burning, non-

28 ferrous metal smelting, coal combustion, ferrous metal smelting, heavy oil combustion, and traffic-
29 related dust changed from 33%, 11%, 15%, 13%, 3%, and 25% to 33%, 8%, 8%, 13%, 4%, and
30 33%, respectively. To date, no significant noncarcinogenic and carcinogenic risks were observed
31 for all of the elements, while both of As and Pb still showed relatively high health damages. It was
32 proposed to further cut down the combustion-related emissions (e.g., As and Pb) because it showed
33 the highest marginal health benefits. Besides, the control of traffic-related emissions might be a key
34 abatement strategy to facilitate the reduction of elements in fine particles.

35 **Keywords:** hourly trace elements; chemical characteristics; health risks; clean air actions; Tangshan

36 1. Introduction

37 Along with the rapid economic development and accelerated urbanization, the energy
38 consumption and output of various industrial products worldwide displayed ~~the~~ persistent increases,
39 thereby leading to ~~the~~ massive emissions of elements especially trace metals into the atmosphere
40 (Tian et al., 2015; Zhu et al., 2020). These elements injected into the atmosphere could pose great
41 ~~threaten~~ to the terrestrial and aquatic ecosystem via dry/wet deposition and then endanger human
42 health through the ~~physicochemicalphysiochemical~~ transfer and bioaccumulation in food chains
43 (Fernandez et al., 2000; Harmens et al., 2010; Storelli, 2008). For instance, some toxic trace metals
44 including cadmium (Cd), lead (Pb), and mercury (Hg) were often regarded as human carcinogens
45 even in trace amounts (Micheline et al., 2019; Olujimi et al., 2015). Besides, the excessive
46 accumulation of some biological essential elements such as copper (Cu), iron (Fe), and zinc (Zn)
47 could initiate activation of inflammatory cascades in tissues and the induction of biochemical
48 synthesis pathways by catalyzing the generation of reactive oxygen species (ROS) (Alies et al., 2013;
49 Lopez-Cruz et al., 2016; Saffari et al., 2014), though minor enrichment of these elements was
50 beneficial to the human health and plant growth (Oldani et al., 2017). Apart from the health impacts,
51 some transition metals (e.g., Ni, Zn) could catalyze some chemical reactions such as particle-phase
52 sulfate generation and heterogeneous production and removal of gas-phase hydrogen oxide radicals
53 (HO_x) to aggravate the haze formation (Clements et al., 2013; Guo et al., 2014). Therefore, it is
54 highly imperative to recognize the pollution status of elements in the atmosphere, to identify the
55 major sources and then to propose effective controls measures to alleviate their negative effects on
56 air pollution and human health especially in some developing countries.

57 In the past decades, hundreds of studies investigated the pollution levels of elements and
58 revealed their sources in various study regions including urban (Das et al., 2018; Duan and Tan,
59 2013; Lyu et al., 2017; [Grivas et al., 2018](#); [Clements et al., 2014](#)), marine (Shi et al., 2015; Witt et
60 al., 2006), ~~mountain~~mountainous (Kang et al., 2016). Most of these studies used ~~the~~-filter sampling
61 (one sample or two samples each day) ~~technique~~-coupled with offline analysis using inductively
62 coupled plasma mass spectrometry (ICP-MS) or inductively coupled plasma-atomic emission
63 spectrometry (ICP-AES) to determine the element concentrations in the atmosphere (Ao et al., 2019;
64 Lin et al., 2016). Although these studies have obtained ~~many-much~~ valuable information about the
65 occurrence levels and key sources of ambient elements, the low time-resolution data cannot
66 accurately reflect the dynamic transformation and evolution of ambient elements. It was well known
67 that atmospheric emissions, transport and deposition significantly relied on rapidly evolving
68 meteorological conditions (Holden et al., 2016; Rasmussen, 1998), and thus the offline samples
69 inevitably ignored the impacts of environmental shifts with rapid temporality on the atmospheric
70 element concentrations. Moreover, most of current source apportionment studies employed ~~the~~
71 receptor models (positive matrix factorization (PMF)) to determine the potential sources of elements
72 (Jeong et al., 2016; Lyu et al., 2017), and the accuracy of these models was strongly dependent on
73 the sample size and time resolution (Liu et al., 2018b). In this regard, the high time-resolved
74 observation of atmospheric elements provided an unprecedented opportunity to characterize the
75 occurrence levels, identify their major sources, and assess the health impacts.

76 To date, only a few studies applied the high-resolution devices to capture the hourly variability
77 of ambient elements. [Prati et al. \(2000\) firstly used Particle Induced X-ray Emission \(PIXE\)](#)
78 [measurements to measure hourly trace elements in Genoa in Italy. Following this work,](#)
79 [D'Alessandro et al. \(2003\) and Dall'Osto et al. \(2013\) also employed the same technique to](#)
80 [determine the trace metals in Italian towns and Barcelona, respectively.](#) Later on, Jeong et al. (2016)
81 used ~~the~~Xact metals monitor to reveal the temporal variability of atmospheric elements in Toronto,
82 Canada in summer and winter during 2013-2014. Recently, the Xact metals monitor has begun to
83 be ~~performed-employed~~ in China due to the higher accuracy and convenience. Chang et al. (2018)
84 firstly used the online multi-element analyzer to achieve a one-year near real-time observation of
85 ambient elements in China and found ~~that~~ traffic, nonferrous metal smelting and coal combustion

86 were major sources of atmospheric trace metals. Afterwards, Cui et al. (2019) applied the analyzer
87 to monitor ~~1-year~~ atmospheric elements during a full year, and demonstrated that dust, industry, and
88 biomass burning were ~~considered as~~ the dominant sources of most trace elements in Beijing,
89 accounting for 36%, 10.7%, and 27% of total PM_{2.5} concentration, respectively. Up to date,
90 continuous hourly element observation was only performed less than one year in most of the
91 previous studies, and the long-term temporal variability of absolute concentrations and key pollution
92 sources of atmospheric elements cannot be fully revealed.

93 Since 2013, Chinese government proposed a strict Air Pollution Prevention and Control Action
94 Plan (the Action Plan) across China and the emissions of multiple gaseous pollutants ~~suffered~~
95 ~~from~~ showed significant decreases. In turn, the absolute concentrations and health effects of air
96 pollutants also experienced the rapid changes response due to these stringent control measures.
97 Zhang et al. (2019) reported that the population-weighted annual mean PM_{2.5} concentration
98 decreased from 62 to 42 µg/m³ during 2013-2017 and reduced PM_{2.5}-attributable premature deaths
99 by 0.4 million due to the impact of the Action Plan. Shortly after that, Geng et al. (2019) estimated
100 that the population-weighted mean concentrations of SO₄²⁻, NO₃⁻, and NH₄⁺ in PM_{2.5} decreased from
101 11.1, 13.8, and 7.4 µg/m³ to 6.7, 13.1, and 5.8 µg/m³, respectively, — during the same period.
102 Nevertheless, the impact of the Action Plan on trace elements in fine particles still remained poorly
103 understood. Especially, the knowledge about the variation of source apportionment and health risks
104 for trace elements response to the Action Plan was extremely limited. Moreover, most of the
105 previous studies only utilized the original concentrations to analyze the impact of the clean air policy
106 (He et al., 2021; Xiao et al., 2020). It was well known that the pollutant concentrations in the
107 atmosphere were affected by meteorology and anthropogenic emissions simultaneously (Li et al.,
108 2021), and the use of original element concentrations alone cannot assess the unique contribution
109 of emission reduction to the air pollutants. Thus, it is urgently needed to remove the effect of
110 meteorology and accurately capture the independent influence of the Action Plan on the chemical
111 characteristics, source apportionment, and health risks of trace elements. Such knowledge is critical
112 to design effective air pollution mitigation strategies in the near future.

113 As a heavily industrialized city located in the North China Plain (NCP), Tangshan possesses
114 many energy-intensive industries including coal-fired power plants, non-ferrous smelting industries,

115 textiles, building materials, chemical engineering, and papermaking industries (Ren et al., 2011).
116 Intensifying industrial development and urbanization aggravated local air quality. Previous studies
117 performed in Tangshan focused on the trace metals in soils and dusts (Cui et al., 2020; Song et al.,
118 2011), whereas no study analyzed the long-term and high-resolution variabilities of atmospheric
119 elements. Since 2013, many emission control measures such as the establishment of desulfurization
120 and denitration facilities for [the](#) coal-fired power sector have been strictly implemented in Tangshan
121 (Ma et al., 2019). Especially after 2017, [the](#) coal to gas project has started to be implemented in
122 Tangshan and the energy structure ~~suffered from~~[underwent](#) significant change (Wang et al., 2020b).
123 In response to substantial pollution control policies, the chemical compositions and major sources
124 of trace elements might show corresponding change. Here, we conducted a near real-time
125 measurement of atmospheric elements in PM_{2.5} using a Xact multi-metals analyzer in Tangshan,
126 China, ~~—~~during September 2017 to August 2020. The primary objectives of our study were to (1)
127 determine the occurrence levels of elements in PM_{2.5} of Tangshan; (2) to analyze the seasonal and
128 intra-week variations of atmospheric elements and to distinguish the separate contributions of
129 emission and meteorology to these species; (3) to quantify the changes of major sources for
130 atmospheric elements during this period; (4) to assess the changes of health risks in response to
131 these pollution control measures.

132 **2. Material and methods**

133 2.1 Sampling site

134 The sampling site (39.66°N, 118.18°E) is situated on the rooftop (~20 m above the ground) of a
135 building in the urban district of Tangshan and no high buildings spread around within 100 m range.
136 The sampling site is close to some major roads including [the](#) Airport Road, Huayan North Road,
137 and Changhong Road. A large number of commercial streets and recreation facility surround the
138 site. Although no big industrial point source was closely adjacent to the sampling site, many
139 potential pollution sources were located more than 15 km away from the site. For instance, [the](#) Beihu
140 industrial region is located about 15 km in the eastern direction of the site. Some large iron steel
141 industries and nonferrous/ferrous smelting industries were located on the north of sampling site
142 (more than 30 km). Besides, most of [the](#) large petrochemical industries, coal-fired power plants, and
143 shipping industries focus on [the](#) Caofeidian and Haigang developing zones, both of which were

144 located about 50 km in the South area of the sampling site. The detailed location is depicted in
145 Figure 1.

146 2.2 Instrumentation

147 Hourly mass concentrations of 22 elements, including Ag, As, Au, Ca, Co, Cu, Cd, Cr, Fe, Ga,
148 Hg, K, Mn, Ni, Pb, Pd, Sb, Se, Sn, Tl, V, and Zn in PM_{2.5} were determined continuously by an online
149 multi-element analyzer (Model Xact 625, Cooper Environment Service, USA) (Table S1). The
150 sample air is drawn through a small spot on the tape where the PM_{2.5} was collected at a flow rate of
151 16.7 L min⁻¹ during September 2017-August 2020. An internal Pd pod is utilized as an internal
152 standard to ~~deteet-determine~~ the stability of the instrument. Tl was removed from the datasets
153 because over 95% of their concentrations were below the limit of detection (LOD) (Table S2). Au,
154 Cd, Sn and Sb were also excluded from the datasets because over 50% of the concentrations for
155 these metals were below the LOD. To validate the reliability of the online multi-element analyzer,
156 many previous studies used the filter sampling coupled with ICP-MS and ICP-AES to determine
157 the daily concentrations of elements and confirmed that the online device showed good agreement
158 with the filter sampling (Furger et al., 2017; Tianxue et al., 2006). Hourly averaged meteorological
159 parameters including air temperature (T), relative humidity (RH), air pressure (P), wind direction
160 (WD), and wind speed (WS) during the sampling period were measured by a weather station with
161 sonic anemometer (150WX, Airmar, Milford, NH, USA). The hourly mass concentration of PM_{2.5}
162 was determined by a particulate monitor (Thermo, FH62C-14). The routine procedures, including
163 the daily zero or standard calibration, span and range check, station environmental control and staff
164 certification, followed the Technical Guideline of Automatic Stations of Ambient Air Quality in
165 Tangshan based on the national specification HJ/T193-2005, which was revised based on the
166 technical guidance established by the US EPA. Quality Assurance and Quality Control (QA/QC) for
167 the Xact measurements was implemented throughout the sampling period. The internal Pd upscale
168 value was recorded after daily programmed test for the instrument.

设置了格式: 下标

169 2.3 Deweathered model development

170 The concentrations of air pollutants were affected by meteorological parameters and emissions
171 simultaneously. In order to separate the contributions of emissions, the impacts of meteorological
172 conditions must be eliminated. In this study, a typical machine-learning model named random forest

173 (RF) approach was applied to distinguish the effects of emissions and meteorological conditions
174 (Chen et al., 2018). All of [the](#) trace elements in PM_{2.5} were treated as the dependent variables. The
175 time predictors (year, day of year (DOY), day of week (DOW), hour of day (HOY)) and
176 meteorological factors including air temperature (T), relative humidity (RH), wind speed (WS),
177 wind direction (WD), and air pressure (P) were regarded as the predictors (Figure S1). The original
178 dataset was randomly classified into a training dataset (80% of input dataset) for developing the RF
179 model and the remained one was treated as the test dataset. After the building of the RF model, the
180 deweathered technique was employed to predict the concentrations of trace elements at a specific
181 time point. The deweathered element concentrations served as the concentrations contributed by
182 emission alone. The differences [between the](#) original element concentrations and [the](#) deweathered
183 element concentrations were regarded as the concentrations contributed by meteorology. Many
184 statistical indicators including R² value, [root-mean-square error \(RMSE\)](#), and [mean absolute error](#)
185 [\(MAE\)](#) were regarded as the major indicators to evaluate the RF modelling accuracy. The RF model
186 with the 5-fold cross-validation R² value less than 0.5 was considered to be [the-an](#) unconvincing
187 result and cannot reflect the impacts of emission and meteorology on air pollutants accurately
188 because more than 50% variability of the training model cannot be appropriately explained. After
189 the model evaluation, only the trace elements with the cross-validation R² values larger than 0.5
190 were selected to estimate the respective contributions of emission and meteorology to the total
191 element concentrations.

192 2.4 PMF model

193 As a typical receptor model applied to source apportionment, [the](#) PMF 5.0 version was used to
194 identify the major origins of [the](#) atmospheric elements and to determine the contribution ratio of
195 each source to these elements ([Norris et al., 2014](#)). The objective of PMF is to solve the issues of
196 chemical mass balance between [the](#) measured concentration of each element and its source
197 contributions by decomposing the input matrix into [factor contributions](#) and [factor profiles](#). The
198 detailed equation is shown in Eq. (1). Besides, the contribution of each source for [an](#) individual
199 element must be non-negative because no sample has a negative source contribution. In brief, the
200 basic principle of PMF is to calculate the least object function Q when the g_{ik} must be a positive-
201 definite matrix based on Eq. (2) (Paatero and Tapper, 1994; Reff et al., 2007).

202

$$x_{ij} = \sum_{k=1}^p g_{ik} f_{kj} + e_{ij} \quad (1)$$

203

$$Q = \sum_{i=1}^n \sum_{j=1}^m \left[\frac{x_{ij} - \sum_{k=1}^p g_{ik} f_{kj}}{u_{ij}} \right]^2 \quad (2)$$

204

205

206

207

208

209

210

211

212

213

214

215

216

217

218

219

220

221

222

223

224

225

226

227

228

where x_{ij} and e_{ij} denote the concentration and uncertainty of the j th element, respectively. g_{ik} represents the contribution ratio of the k th source to the i th sample, f_{kj} represents the ratio of the j th element in the k th source, and e_{ij} indicates the residual of the j th element in the i sample. The uncertainties associated with factor profiles were evaluated using three error calculation methods including the bootstrap (BS) method, displacement (DISP) analysis, and the combination method of DISP and BS (BS-DISP). For the BS method, 100 runs were performed and the result has been believed to be valid since all of the factors showed a mapping of above 90%. DISP analysis also confirmed that the solution was considered to be stable because the observed drop in the Q value was less than 0.1% and no factor swap occurred. For the BS-DISP analysis, the solution has been verified to be useful because the observed drop in the Q value was less than 0.5%. Furthermore, both of the results from BS and BS-DISP did not suggest any asymmetry or rotational ambiguity for all of the factors (Manousakas et al., 2017; Taghvaei et al., 2018).

2.5 Health risk assessment of trace metals in PM_{2.5}

As a typical industrial city, Tangshan possesses a large number of residents and poor air quality. Therefore, the residents in Tangshan might suffer from severe exposure risks of trace metals. In our work, the carcinogenic and non-carcinogenic risks of trace metals in PM_{2.5} were evaluated based on some statistical threshold proposed by the International Agency for Research on Cancer (IARC). Based on the criterion of the IARC, As, Ni, Cr, and Pb were considered to be carcinogenic to humans.

The carcinogenic and non-carcinogenic risks induced by ~~meatal-metal~~ exposure for adults and children were evaluated based on the carcinogenic risks (CR) and hazard quotient (HQ). The formulas for calculating ADD, CR, and HQ are as follows:

$$ADD = (C \times InhR \times EF \times ED) / (BW \times AT) \quad (3)$$

$$HQ = ADD / RfD \quad (4)$$

$$CR = ADD \times CSF \quad (5)$$

where C (mg m^{-3}) denotes the concentration of the corresponding trace metal in PM_{2.5}; $InhR$ is the

229 respiratory rate; EF represents the annual exposure frequency (d y^{-1}); ED is the exposure duration
230 (year); BW is the average body weight (kg); AT denotes the average exposure time (d); ADD means
231 the daily intake (mg/kg/day) of trace metals; RfD represents the reference dose ($\text{mg kg}^{-1} \text{d}^{-1}$),
232 calculated with reference concentrations; CSF is the cancer slope factor (kg d/mg). The potential
233 non-carcinogenic risk of the trace metal is considered to be might be high when HQ was above 1.0,
234 whereas the health risk is not obvious when HQ is below 1.0. The carcinogenic risk of each trace
235 metal is evaluated based on whether CR is higher than 10^{-4} .

236 3. Results and discussion

237 3.1 Occurrence levels and inter-annual variations of original element concentrations

238 The total mass concentrations of 16 elements in $\text{PM}_{2.5}$ of Tangshan varied between 230 ng/m^3
239 to 20000 ng/m^3 , with the median-average value (\pm standard deviation) of $3100 \pm 900 \text{ ng/m}^3$. The
240 total element concentrations in Tangshan accounted for 5.7% of the total mass concentrations of
241 $\text{PM}_{2.5}$, which was slightly higher than those in Beijing (4.7%) and Qingdao (4.0%), and significantly
242 higher than that in Shanghai (1.80%) (Chang et al., 2018; Cui et al., 2019). As depicted in Figure 2,
243 the concentrations of these elements followed the order of $\text{K} (1400 \pm 950 \text{ ng/m}^3) > \text{Fe} (880 \pm 590$
244 $\text{ ng/m}^3) > \text{Ca} (330 \pm 270 \text{ ng/m}^3) > \text{Zn} (320 \pm 160 \text{ ng/m}^3) > \text{Pb} (58 \pm 36 \text{ ng/m}^3) > \text{Mn} (54 \pm 32 \text{ ng/m}^3) >$
245 $\text{Cu} (22 \pm 19 \text{ ng/m}^3) > \text{As} (15.3 \pm 11.0 \text{ ng/m}^3) > \text{Se} (6.5 \pm 5.3 \text{ ng/m}^3) > \text{V} (4.0 \pm 3.6 \text{ ng/m}^3) > \text{Cr} (2.8$
246 $\pm 2.2 \text{ ng/m}^3) > \text{Ag} (2.8 \pm 2.1 \text{ ng/m}^3) > \text{Ni} (2.2 \pm 1.8 \text{ ng/m}^3) > \text{Hg} (1.5 \pm 0.8 \text{ ng/m}^3) > \text{Ga} (0.9 \pm 0.7$
247 $\text{ ng/m}^3) > \text{Co} (0.7 \pm 0.2 \text{ ng/m}^3)$. Among all of these elements, K, Fe, Zn, and Ca were the most
248 abundant species, accounting for 95% of the total elements in $\text{PM}_{2.5}$. The remaining element
249 concentrations only accounted for less than 6% of the total element concentrations, which was
250 similar to the-in previous studies (Chang et al., 2018; Cui et al., 2019). Nearly all of the trace
251 elements in Tangshan, Beijing, Qingdao, and Shanghai were significantly lower than those in Zibo
252 during 2006-2007 (Table S3). It suggested that the trace elements in China experienced marked
253 decreases in the past decades (Zhang et al., 2018). Compared with some cities in some developed
254 countries, all of the trace element concentrations were significantly higher than those in London and
255 Toronto. Moreover, the concentrations of K, Ca, V, Cr, Mn, and Fe in Tangshan were higher than
256 those in Venice, Italy.

257 Due to the higher exposure risk and great threaten to human health, it is necessary to compare

258 the trace metal concentrations with the risk threshold proposed by many organizations or countries.
259 As shown in Table 1, we have collected many risk thresholds in different countries and found that
260 the Hg ($1.5 \pm 0.8 \text{ ng/m}^3$), Ni ($2.2 \pm 1.8 \text{ ng/m}^3$), and Pb concentrations ($58 \pm 36 \text{ ng/m}^3$) in Tangshan
261 were significantly lower than the thresholds of the Chinese Ambient Air Quality Standard (CAAQS)
262 (Hg: 50 ng/m^3), World Health Organization (WHO) (Hg: 1000 ng/m^3 , Ni: 25 ng/m^3 , and Pb: 1000
263 ng/m^3), European Union (EU) (Ni: 20 ng/m^3), and the United States (Pb: 150 ng/m^3). However, both
264 of the As ($15 \pm 11 \text{ ng/m}^3$) and Cr concentrations ($2.8 \pm 2.2 \text{ ng/m}^3$) in PM_{2.5} of Tangshan were much
265 higher than the standard values of the CAAQS (As: 6.0 ng/m^3 and Cr: 0.03 ng/m^3), WHO (As: 6.6
266 ng/m^3 and Cr: 0.25 ng/m^3), and EU (As: 6.0 ng/m^3).

267 The inter-annual variation of the original concentrations of trace elements in PM_{2.5} are depicted
268 in Figure 3 and S2-S3. The original concentrations of all the trace elements exhibited the decreasing
269 trends. Cu, Co, Zn, Pb, As, and Ga concentrations ~~suffered from~~ showed dramatic decreases from
270 37 to 12 ng/m^3 (68%), 1.21 to 0.4 ng/m^3 (66%), 400 to 190 ng/m^3 (53%), 71 to 40 ng/m^3 (44%), 20
271 to 11 ng/m^3 (44%), and 1.09 to 0.6 ng/m^3 (42%), respectively. Following these species, ~~observed~~
272 the K (40%), Ag (39%), V (39%), Ni (36%), Ca (33%), Mn (29%), Se (29%), Fe (27%), and Cr
273 (21%) concentrations showed moderate decreasing ratios. The observed Hg level exhibited the
274 lowest decreasing ratio from 1.59 to 1.43 ng/m^3 (9.9%).

275 3.2 Impact of emission reduction on trace element concentrations

276 Although the original concentrations of the trace elements could be utilized to analyze the impact
277 of the clean air policy, the role of emission reduction on the element concentration might not be
278 clearly clarified because the meteorological factors were also important variables affecting the air
279 quality. In order to accurately reflect the response of the element concentrations to the emission
280 reduction alone during 2017-2020, the meteorological conditions were eliminated by the RF model
281 in our study. Based on the results in Figure S4, the RF models for all of the species showed better
282 performance because their R² values were higher than 0.50, and the slopes of all of the fitting curves
283 were also close to the R² values. The result suggested that the separation of meteorology and
284 emission of trace elements based on the RF model was reliable. During 2017-2020, the deweathered
285 concentrations of Ga, Co, Pb, Zn, and As showed the rapid decreases from 1.52 to 0.4 ng/m^3 (72%),
286 1.31 to 0.4 ng/m^3 (67%), 92 to 35 ng/m^3 (62%), 410 to 170 ng/m^3 (59%), and 21 to 10 ng/m^3 (54%),

287 respectively (Figure 3). It was well known that As, Co, and Pb were typical marker elements for
288 coal combustion and the “coal-to-gas” and “coal-to-electricity” strategies have been widely
289 performed in Tangshan (Fang et al., 2020; Li et al., 2017). Wang et al. (2020a) ~~has~~ ~~have~~ estimated
290 that these effective control measures have contributed to around 60% of the total PM_{2.5} reductions.
291 Meanwhile, the upgradation and optimization of ~~the~~ industrial structure/layout and the shutdown of
292 high-pollution industries were also strictly implemented in Tangshan, and thus led to the dramatic
293 decreases of Ga and Zn concentrations because Ga and Zn were common forms of nonferrous metal
294 smelting (Tian et al., 2015). ~~However~~ ~~In contrast~~, the deweathered Ca level displayed the lowest
295 decrease ratio (8.3%) from 2017 to 2020, indicating that clean air actions cannot significantly reduce
296 the fugitive emissions. In addition, the deweathered Fe (23%) and Cr (18.5%) also suffered from
297 relatively low decrease ratios. It was well documented that Fe and Cr originated from metallurgical
298 industry such as steel production and ferrous metal smelting (Tian et al., 2015), and the slight
299 decreases of ~~the~~ deweathered Fe and Cr levels during the sampling period suggested that the
300 emission control measures for ferrous metal smelting should be strengthened in the future ~~work~~.

301 In addition, the decreasing ratios of the deweathered concentrations for each species displayed
302 different seasonal characteristics. The deweathered concentrations of some elements related with
303 industrial activities (e.g., Ga, Zn, and Cr) ~~suffered from~~ ~~showed~~ rapid decreases in autumn and winter
304 compared with other seasons during 2017-2020 (Figure 4), indicating that the optimization of ~~the~~
305 industrial layout and shutdown of outdated industries were effective to decrease these element
306 emissions especially in ~~the~~ high-pollution season. Some elements derived from biomass burning
307 including K (66%) and Se (50%) also ~~exhibited~~ ~~suffered from~~ the most dramatic decreasing ratios
308 in autumn. It was assumed that enhanced crop residual burning occurred frequently during the
309 autumn harvest season. ~~Ke et al. (2019) confirmed that the number of fire spots in October-~~
310 ~~November was even higher than that in June and the burned area in the harvest season was highest~~
311 ~~during 2013-2017~~. However, the control on open biomass burning has been implemented strictly in
312 recent years, largely reducing the K and Se emissions in autumn. It should be noted that the
313 deweathered Pb (46%), Co (65%), and As (45%) concentrations in winter did not display high
314 decreasing ratios though the annual mean deweathered Pb, Co and As levels experienced dramatic
315 decreases. The result revealed that it was still difficult to reduce the Pb, Co, and As emissions during

316 the heating season because increased coal consumption for domestic heating largely offset the
317 contributions of emission control measures (Zhu et al., 2018; Zhu et al., 2020).

318 Apart from the seasonal difference of each species, the decreasing ratios of these elements also
319 suffered from distinctly intra-weekly variations. The deweathered concentrations of most elements
320 except Ca, Cu, Ni, and V exhibited ~~the~~ higher decreasing ratios at the weekends than ~~those in~~ the
321 weekdays (Figure 5). Cui et al. (2020) ~~has~~ ~~have~~ demonstrated that the weaker supervision on
322 industrial enterprises on weekends could lead to the higher concentrations of non-traffic elements
323 such as K, As, Se, and Cr in some cities. Fortunately, grid monitoring has been widely performed
324 in Tangshan recently
325 (<http://hbepb.hebei.gov.cn/hbhjt/xwzx/jicengfengcai/101624062321621.html>), and many low-cost
326 sensors were installed at some energy-intensive industries, which could decrease the stealing
327 emissions of some elements. Nonetheless, the decreasing ratios of Ca, Cu, V, and Ni did not show
328 the regular intra-weekly characteristics. In recent years, Tangshan adopted strict traffic management
329 regulation and the nonlocal light duty vehicles were restricted to drive inside the urban area one day
330 per week based on the end number of the license plates (Westerdahl et al., 2009; Wu et al., 2011),
331 whereas the restrictions were not valid at weekends (Liu et al., 2007). Theoretically, the traffic
332 control should result in marked decreases of traffic-related element concentrations on weekdays
333 compared with weekends. However, in our study, some traffic-related elements such as Ca and Cu
334 did not show similar characteristics. Meanwhile, as the important tracer of vehicle emission, the
335 NO_x concentration in Tangshan did not show a regular intra-weekly pattern. It was supposed that
336 the vehicle volume in Tangshan has increased from 2.0 to 2.4 million (<http://tjj.hebei.gov.cn/>),
337 which largely offset the benefits of traffic controls. The shipping-related elements including V and
338 Ni also did not show regular intra-weekly variation because no ~~similar~~ ~~heavy metal~~ emission control
339 measures for shipping were performed.

340 3.3 The role of meteorology on the year-to-year variations of element concentrations

341 The difference ~~of between the~~ original and deweathered element concentrations could be regarded
342 as the concentrations contributed by meteorological parameters. The positive impacts of
343 meteorological parameters on ~~the~~ trace elements suggested that the meteorological conditions were
344 unfavorable to the pollutant diffusion, while the negative impacts of meteorological indicators

设置了格式: 下标

345 meant the favorable condition to trace elements. In our study, the roles of meteorological conditions
346 on Ca (-25%), V (-10%), Cr (-2.5%), Mn (-0.7%), Fe (-4.6%), Ni (-7.6%), and Cu (-21%) during
347 2017-2020 were negative (Figure S5), while the roles of meteorological parameters on other
348 elements were positive. The result suggested that those elements derived from vehicle emission (Ca,
349 Cu, and Fe), ferrous metal smelting (Cr and Mn), and heavy oil combustion (V and Ni) were less
350 sensitive to the emission reduction actions compared with other elements and the meteorological
351 conditions were much beneficial to the diffusion of these elements. In order to further reveal the key
352 meteorological factors for these elements, we used [the RF](#) model to calculate the variable
353 importance of all of these meteorological parameters including P, RH, T, WD, and WS. The result
354 suggested that Ca, Fe, and Cu were mainly influenced by T, whereas V, Ni, Cr, and Mn were often
355 associated with WD and WS (Figure 6). During [the spring and summer in 2017-2020](#), the average
356 air temperature [decreased from 8.9 and 27 to 7.2 and 26°C, respectively](#). The [decreased](#) air
357 temperature [led to a higher water content in the soil and a lower tendency of dust suspension](#), and
358 might decrease the concentrations of Ca, Fe, and Cu (Manju et al., 2018; Yang et al., 2017; [Lyu et](#)
359 [al., 2016](#)). Although the annual average wind speed in Tangshan decreased from 1.70 to 1.45 m/s,
360 the mean wind speed from the southeastern direction displayed [a slight increase](#) from 1.34 to 1.50
361 m/s. Zhao et al. (2013) verified that V and Ni were usually emitted from heavy oil combustion of
362 ocean-going ship engines. Many coastal ports and ferrous metal smelting industries were located on
363 the southeastern direction of the sampling site, and thus the enhanced WS [might promote](#) the
364 dilution and dispersion of trace elements ([Figures S6-S8](#)). [As shown in Figure S8, both of V and Ni](#)
365 [showed the higher concentrations in the southeastern part of Tangshan and the concentrations](#)
366 [displayed gradual decreases along the Southeast-Northwest transect, which also demonstrated that](#)
367 [both of V and Ni in the sampling site could be derived from coastal shipping emission](#).

368 3.4 The impact of clean air policy on [the](#) source apportionment of trace elements

369 Although the major sources of elements could be determined based on some important tracers
370 (e.g., K, V), the contributions of [the](#) major sources to each element still remained unknown.
371 Therefore, Positive matrix factorization ([version](#) PMF 5.0) ~~version~~ was applied to identify more
372 source information of [the](#) elements in PM_{2.5} during 2017-2020 based on [the](#) deweathered levels.
373 After 20 runs, more than 26000 samples were trained to determine the optimal six factors with the

374 lowest values of Q (robust) and Q (true). The BS, DISP, and BS-DISP methods confirmed that the
375 most reliable solution was obtained with six factors. The detailed information of the PMF analysis
376 and error diagnostics are is summarized in Table S4-S6.

377 As shown in Figure S9, the trace elements in PM_{2.5} during 2017-~~2018, 2018-2019, and 2019-~~
378 2020 showed similar eluster-characteristics. Factor 1 possesses high loadings of K (55%) and Se
379 (42%). K and Se were often regarded as the major tracers of biomass burning. Due to the increasing
380 usage of biomass fuels for domestic heating during the heating season, K_r and Se in PM_{2.5} of
381 Tangshan showed the higher values in winter, suggesting that these metals in fine particles could
382 originate from the combustion of biomass fuels. Except for the domestic heating, we found some
383 episodes during the harvesting season in late summer (2500 and 11.2 ng/m³) and early autumn (2600
384 and 9.5 ng/m³) also showed extremely high concentrations of K, which might be linked with local
385 open-biomass burning (Chen et al., 2017). Based on the map of fire points and backward air masses
386 trajectories (Figures ~~S7S6-S8~~), the metals released from biomass burning or open waste incineration
387 in the NCP could be transported to the sampling site by the dominant southerly wind, which further
388 proved the impacts of open-biomass burning (Chen et al., 2017).

389 The abundant elements in factor 2 included Ag (53%), Zn (51%), and Cu (36%). Owing to the
390 higher temperatures during the roasting, sintering and smelting processes for the extraction of Cu,
391 and Zn from ores, some metals such as Ag in nonferrous metal ores could be vaporized as the a
392 byproduct and released into the flue gas (Pacyna and Pacyna, 2001; Wu et al., 2012). Therefore, the
393 factor 2 was interpreted as the non-ferrous metal smelting source.

394 Factor 3 was characterized by a large mass fraction of Co (81%), Pb (61%), Hg (57%), and As
395 (39%). After the phase-out of leaded gasoline since 1980s, the contribution from coal combustion
396 to Pb suffered from showed rapid increase and accounted for the major fraction of particulate Pb
397 (Das et al., 2018). Meanwhile, Co and Hg were also treated as the important byproducts released
398 from coal burning and the Co and Hg concentrations often increased significantly with the elevation
399 of the burning temperature (Tang et al., 2018). Tian et al. (2015) estimated that 73% of As, 56 % of
400 Pb, and 47 % of Hg were found to be emitted from coal combustion in China. Coal consumption in
401 South China was mainly driven by coal-fired power plants, while the coal-based heating was the
402 major sector for the coal consumption in the NCP. In our study, As, Co and Pb showed the higher

设置了格式: 上标

设置了格式: 上标

403 concentrations in winter (heating season) (18.7, 0.9, and 76 ng/m³) compared with other seasons
404 (14, 0.6, and 51 ng/m³). The markedly seasonal discrepancies of As, Co and Pb strongly supported
405 the impact of the coal combustion for domestic heating on the enhancement of As, Co and Pb in the
406 fine particles.

407 Factor 4 was distinguished by high loadings of Cr (78%) and Mn (39%), respectively. Cr and
408 Mn were mainly sourced-originated from metallurgical industry such as steel production and ferrous
409 metal smelting (Liu et al., 2018a; Tian et al., 2015; Zhu et al., 2018). China was responsible for
410 more than 49% of the world steel production in 2017 (approximate 830 million tons), and 60% of
411 the large steel producers were located in China (Chang et al., 2018). Tangshan possesses many large
412 steel production industries such as Tangshan Steel, Qian'an Steel, and Guofeng Steel. Besides, some
413 industries of Capital Steel have been migrated into Tangshan (Li et al., 2019), which might increase
414 the Cr and Mn emissions.

415 Factor 5 explained 10.1% of the total species and it was characterized by high loadings of V
416 (88%) and Ni (51%). It was well documented that V was a key fingerprint of heavy oil combustion,
417 which was generally emitted from shipping emission and petrochemical refining (Shafer et al.,
418 2012). However, Ni was widely utilized as a tracer of fuel oil combustion in industries (Zhu et al.,
419 2018). Many oil-fired power plants were located in Tangshan for central heating (Yu et al., 2013).
420 Based on the backward trajectory and wind direction (Figures S7S6-S10S8), we found that high
421 concentrations of V and Ni might be derived from the southeastern air masses especially in summer
422 and autumn, indicating the impacts of coastal port and petroleum refinery industry. In addition, the
423 V and Ni concentrations displayed the gradual decreases along the Southeast-Northwest transect,
424 indicating the potential sources were located on Southeast Tangshan (Figure S8). Gathering
425 evidence suggested that the V/Ni ratio in petroleum coke with a low-sulfur content and fuel oil
426 usage ranged from 1 to 3 (Moreno et al., 2010). The annual mean ratios of V and Ni in our study
427 reached 1.2 during the sampling period, which was in the range of this interval. The result also
428 revealed that petrochemical refining and heavy oil combustion derived from coastal shipping
429 emission might be an important source of V and Ni in the fine particles.

430 Factor 6 was characterized by high loadings of Ca (78%), Cu (32%), and Fe (33%), and moderate
431 loadings of Mn (31%) and Zn (29%). Some previous studies have demonstrated that both of Cu, Fe,

432 and Zn were released from tyre and brake wear because they were the necessary materials for brake
433 pads and the agents in brake linings (Dall'Osto et al., 2013; Hjortenkrans et al., 2007). Ca ~~was~~
434 probably ~~sourced~~originated from the road fugitive dust because it was one of the most abundant
435 elements in the upper ~~continents~~soil (Alves et al., 2015; Liu et al., 2018a). Moreover, we have
436 found Fe, Ca, and Zn displayed remarkably high values during the morning rush hours and a small
437 peak during the sunset (Figure S10), which was coincident to the diurnal variation of the traffic
438 volume. Thus, the factor 6 was identified as the traffic-related dust source.

439 Although six similar sources were revealed during 2017-2020, the contribution concentrations
440 and ratios of these sources varied greatly in these years. As shown in Figures 7 and 8, the
441 contribution concentrations of biomass burning, non-ferrous metal smelting, coal combustion, and
442 ferrous metal smelting to trace elements decreased from 1460, 480, 640, and 570 ng/m³ to 900, 230,
443 230, and 350 ng/m³, respectively. However, the contribution concentrations of heavy oil combustion
444 and traffic-related dust displayed a slight increase during 2017-2019, while they decreased rapidly
445 after 2019. The contribution concentrations for nearly all sources to trace elements suffered from
446 decreases during 2017-2020 because the total deweathered levels of trace elements experienced
447 decreases in the past three years. However, the contribution ratios of these sources to the trace
448 elements did not show similar characteristics. For instance, the contribution ratio of the traffic-
449 related dust increased from 25% to 33%. In contrast, the contributions of non-ferrous metal smelting
450 and coal combustion decreased from 11% to 8% and 15% to 8%, respectively. The contributions of
451 ferrous metal smelting, heavy oil combustion, and biomass burning remained relatively stable
452 during this period.

453 Due to the strict implementation of the clean air policy, many outdated industrial capacities were
454 shut down and cleaner technologies have been upgraded, which facilitated the production decreases
455 of pig iron and coal-fired power plants (Ma et al., 2019). Hence, the contribution concentrations and
456 ratios of non-ferrous metal smelting and coal combustion experienced dramatic decreases. Although
457 the open biomass burning has been strictly restricted in Tangshan (Chang et al., 2018), the
458 contribution ratios of biomass burning to the trace elements in PM_{2.5} remained relatively stable,
459 which might be attributable to the rapid decreases of the contributions derived from coal combustion
460 and non-ferrous metal smelting. In addition, the biofuel combustion was still widespread in some

461 rural and suburb areas (Kamal et al., 2015; Li et al., 2020), which might offset the decreases in the
462 contributions of open biomass burning. Although the contribution concentrations of traffic-related
463 dust to trace elements also showed slight decrease, the contribution ratios of traffic-related dust to
464 some trace elements exhibited marked increases (8%) during 2017-2020 because the contribution
465 ratios of metal smelting and coal combustion displayed substantial decreases. The result also
466 demonstrated that the implementation of coal to gas project facilitated the decreases of trace element
467 concentrations. In addition, the source variation trend also suggested that the formulation of many
468 new quality standards for non-road diesel fuels cannot fully decrease the element emissions (Cui et
469 al., 2017), and thus the control of traffic-related dust should be enhanced in the future.

470 3.4.5 Health risk assessment of trace metals in PM_{2.5}

471 Although the trace metals only accounted for a minor fraction of the total mass concentration of
472 PM_{2.5}, it might pose a great threat to the human health because most of these metals were
473 bioavailable and non-degradable (Rai et al., 2019; Yi et al., 2011). Unfortunately, previous studies
474 mainly used the filter sampling techniques to determine the concentrations of trace metals and then
475 assess their health risks (Cui et al., 2018; Huang et al., 2016). These low-resolution data might not
476 accurately reflect the real health risks triggered by metal exposure. In our study, we employed the
477 online data to assess the health risks derived from metal exposure.

478 The health risks of trace metals could be classified into two types including carcinogenic and
479 non-carcinogenic risk. Based on the major parameters summarized in Tables S7 and Table S8, we
480 estimated both of the carcinogenic and non-carcinogenic risks of the major metals. To evaluate the
481 impacts of emission control measures on the element concentrations, both of the health risks based
482 on original element levels and the deweathered element concentrations were calculated. The mean
483 CR values based on the original concentrations were in the order of Pb (2.3×10^{-6} (adult) and 1.4×10^{-6}
484 (child)) > As (1.9×10^{-6} and 1.1×10^{-6}) > Cr (0.11×10^{-6} and 0.07×10^{-6}). The total CR values for adults
485 and children reached 4.3×10^{-6} and 2.6×10^{-6} (Table 2), respectively. The total CR values were located
486 in the range of the acceptable (10^{-6}) and least stringent risk levels (10^{-4}), which suggested that
487 Tangshan suffered from a slight metal carcinogenic risk. Among all of these metals, Pb and As
488 displayed the higher CR values. It was assumed that the coal combustion for domestic heating might
489 be the dominant factor for the higher risks of Pb and As in Tangshan because both of Pb and As in

490 PM_{2.5} were mainly derived from coal combustion. With regard to the non-carcinogenic risks of the
491 trace metals, the HQ of As (1.2×10^{-2} and 2.9×10^{-2}) and Pb (6.8×10^{-4} and 17×10^{-4}) showed ~~the~~ higher
492 values compared with other elements. The result indicated that nearly all ~~of the~~ elements did not
493 display ~~potential remarkable~~ non-carcinogenic risk because the HQ values of all the metals were
494 less than 1. The total HQ value of these metals ~~were-was~~ also lower than 1, indicating that the trace
495 elements in Tangshan did not show a significant non-carcinogenic risk.

496 By removing the impact of the meteorological conditions, we can isolate the impact of the clean
497 air policy on health risks associated with metal exposure alone. The decrease ratios of the CR values
498 based on the deweathered As and Pb concentrations during 2017-2020 were 54% and 62%,
499 respectively (Table 3). However, the decrease ratios of the CR values based on the original As and
500 Pb levels only reached 44%. The result suggested that the clean air policy in recent years
501 significantly decreased the As and Pb emissions. Additionally, the decrease ratios of HQ values for
502 the original Cu (41%) and Zn (53%) were much less than those for the deweathered ones (Cu: 47%
503 and Zn: 59%). Nevertheless, some other elements did not show ~~the~~ similar characteristics. For
504 instance, the decreased ratios of the HQ values for the original Cr (21%) and Fe (27%) were even
505 slightly higher than those for the deweathered ones (Cr: 19% and Fe: 23%). It was assumed that the
506 clean air policy in recent years facilitated the emission reduction of non-ferrous metal smelting and
507 coal combustion efficiently. However, the concentrations of the elements derived from ferrous metal
508 smelting and vehicle emission did not show marked decreases, which was in good agreement with
509 the source apportionment result in ~~the~~ section 3.3. Thus, in the future work, it is highly imperative
510 to further reduce the industrial/traffic-related emissions in order to alleviate potential health risks.

511 3.6 Limitations and uncertainties

512 It should be noted that our work is still subject to some limitations. At first, some elements
513 such as Cr (0.5) and Ga (0.5) showed relatively lower CV R_x^2 values though they were generally
514 higher than 0.5. These elements might show the higher uncertainties during the meteorology-
515 normalization compared with other elements such as Cu (0.85) and K (0.85). Besides, few variables
516 were applied to deweather the element concentrations, which might be responsible for the lower CV
517 R_x^2 value for some elements. Due to the lack of available hourly emission inventory of each element,
518 we only used the time variable to train the model. This method still suffered from some uncertainties.

带格式的: 缩进: 首行缩进: 2 字符

设置了格式: 上标

设置了格式: 上标

519 ~~which should be improved by the establishment of near-time emission database.~~

520 **4. Conclusions and implications**

521 Three-year continuous hourly observation of elements in PM_{2.5} was conducted in Tangshan
522 during September 2017-August 2020. The effect of ~~air~~-the clean air policy on the element
523 concentrations in PM_{2.5} ~~were~~-was quantified. The main conclusions were drawn as follows:

524 (1) The deweathered concentrations of Ga, Co, Pb, Zn, and As showed ~~the~~ rapid decreases from
525 1.52 to 0.42 ng/m³ (72%), 1.31 to 0.44 ng/m³ (67%), 92 to 35 ng/m³ (62%), 411 to 170 ng/m³
526 (59%), and 21 to 10 ng/m³ (54%), respectively. ~~Clean~~-The clean air actions played the important
527 role on the emission reduction of coal combustion and non-ferrous metal smelting.

528 (2) The deweathered levels of Ca (8.3%), Cr (19%), and Fe (23%) displayed relatively low
529 decreases compared with other elements, indicating that the vehicle emission and ferrous-
530 smelting industries might ~~be not~~not be sensitive to the air clean policy.

531 (3) The deweathered levels of some elements related with industrial activities (e.g., Ga, Zn, and Cr)
532 exhibited rapid decreases in autumn and winter compared with other seasons during 2017-2020,
533 while the combustion-related elements such as Pb and As did not show high decreasing ratios
534 in winter. The enhanced coal consumption during the heating season ~~offsets~~ the benefits derived
535 from strict emission controls measures.

536 (4) The favorable meteorological conditions promoted the decreases of Ca (-25%), V (-10%), Cr (-
537 2.6%), Mn (-0.68%), Fe (-4.6%), Ni (-7.6%), and Cu (-21%) concentrations.

538 (5) The contribution ratios of biomass burning, non-ferrous metal smelting, coal combustion,
539 ferrous metal smelting, heavy oil combustion, and traffic-related dust changed from 33%, 11%,
540 15%, 13%, 3%, and 25% to 33%, 8%, 8%, 13%, 4%, and 33%, respectively.

541 (6) All ~~of the~~ elements did not show significant noncarcinogenic and carcinogenic risks, while both
542 ~~of~~ As and Pb still displayed relatively high health damages.

543 Our study presented detailed information about the impact of clean air policy on the chemical
544 compositions and source apportionment of trace elements in PM_{2.5} in Tangshan, and provided new
545 ~~enlightenment insights~~ for the scientific community and policymakers. Many targeted measures
546 could be undertaken to alleviate the air pollution and further to reduce avoided premature health
547 risks. However, this study still suffered some limitations and more steps will be taken toward

548 thoroughly addressing these problems. First of all, the PMF model still showed some uncertainties,
549 and thus characterizing the isotopic signatures of these elements is of great significance. In addition,
550 a Sunset OC/EC analyzer, a Monitoring of Aerosols and Gases (MARGA) platform, and other on-
551 line measurements should be collocated to probe into the synergistic effect of emission reduction
552 and meteorology on air quality.

553 **Acknowledgements**

554 This work was supported by the National Natural Science Foundation of China (42107113).

555 **Data availability**

556 The boundary layer height dataset was obtained from the website of <https://www.ecmwf.int/>. The
557 dataset is archived in <https://zenodo.org/record/7031975#.Ywys8cjfmfU> (Li et al., 2022).

558 **Author contributions**

559 LR wrote the manuscript. LR, PM, ZWD, and HJM contributed to the conceptualization of the study.

560 LR and PM conducted the research, and visualized the results. WGH revised the manuscript.

561 **Competing interests**

562 The contact authors ~~has~~ have declared that neither they nor their co-authors have any competing
563 interests.

564 **References**

- 565 Alies, B., Sasaki, I., Proux, O., Sayen, S., Guillon, E., Faller, P., and Hureau, C.: Zn impacts Cu
566 coordination to amyloid- β , the Alzheimer's peptide, but not the ROS production and the associated
567 cell toxicity, *Chem. Commun.*, 49, 1214-1216, 2013.
- 568 Alves, C., Gomes, J., Nunes, T., Duarte, M., Calvo, A.I., Custodio, D., Pio, C., Karanasiou, A., and
569 Querol, X.: Size-segregated particulate matter and gaseous emissions from motor vehicles in a road
570 tunnel, *Atmos. Res.*, 153, 134-144, <https://doi.org/10.1016/j.atmosres.2014.08.002>, 2015.
- 571 Ao, M., Qiu, G., Zhang, C., Xu, X., Zhao, L., Feng, X., Qin, S., and Meng, B.: Atmospheric deposition
572 of antimony in a typical mercury-antimony mining area, Shaanxi Province, Southwest China, *Environ.*
573 *Pollut.*, 245, 173-182, <https://doi.org/10.1016/j.envpol.2018.10.125>, 2019.
- 574 Chang, Y., Huang, K., Xie, M., Deng, C., Zou, Z., Liu, S., and Zhang, Y.: First long-term and near real-
575 time measurement of trace elements in China's urban atmosphere: temporal variability, source
576 apportionment and precipitation effect, *Atmos. Chem. Phys.*, 18, 11793-11812,
577 <https://doi.org/10.5194/acp-18-11793-2018>, 2018.
- 578 Chen, J., Li, C., Ristovski, Z., Milic, A., Gu, Y., Islam, M.S., Wang, S., Hao, J., Zhang, H., and He, C.: A
579 review of biomass burning: Emissions and impacts on air quality, health and climate in China, *Sci.*
580 *Total Environ.*, 579, 1000-1034, <https://doi.org/10.1016/j.scitotenv.2016.11.025>, 2017.
- 581 Chen, G.B., Li, S.S., Knibbs, L.D., Hamm, N.A.S., Cao, W., Li, T.T., Guo, J.P., Ren, H.Y., Abramson,
582 M.J., and Guo, Y.M.: A machine learning method to estimate PM_{2.5} concentrations across China with
583 remote sensing, meteorological and land use information, *Sci. Total Environ.*, 636, 52-60,
584 <https://doi.org/10.1016/j.scitotenv.2018.04.251>, 2018.
- 585 Clements, A.L., Buzcuguvan, B., Fraser, M.P., Kulkarni, P., and Chellam, S.: Role of particulate metals
586 in heterogenous secondary sulfate formation, *Atmos. Environ.*, 75, 233-240,
587 <https://doi.org/10.1016/j.atmosenv.2013.04.038>, 2013.
- 588 [Clements, N., Eav, J., Xie, M., Hannigan, M. P., Miller, S. L., Navidi, W., et al.: Concentrations and
589 source insights for trace elements in fine and coarse particulate matter, *Atmos. Environ.*, 89, 373-381,
590 <https://doi.org/10.1016/j.atmosenv.2014.01.011>, 2014.](https://doi.org/10.1016/j.atmosenv.2014.01.011)
- 591 Cui, L., Duo, B., Zhang, F., Li, C., Fu, H., and Chen, J.: Physiochemical characteristics of aerosol
592 particles collected from the Jokhang Temple indoors and the implication to human exposure, *Environ.*
593 *Pollut.*, 236, 992-1003, <https://doi.org/10.1016/j.envpol.2017.10.107>, 2018.
- 594 Cui, M., Chen, Y., Feng, Y., Li, C., Zheng, J., Tian, C., Yan, C., and Zheng, M.: Measurement of PM and
595 its chemical composition in real-world emissions from non-road and on-road diesel vehicles, *Atmos.*
596 *Chem. Phys.*, 17, 6779-6795, <https://doi.org/10.5194/acp-17-6779-2017>, 2017.
- 597 Cui, X., Wang, X., and Liu, B.: The characteristics of heavy metal pollution in surface dust in Tangshan,
598 a heavily industrialized city in North China, and an assessment of associated health risks, *J. Geochem.*
599 *Explor.*, 210, 106432, 2020.
- 600 Cui, Y., Ji, D., Chen, H., Gao, M., Maenhaut, W., He, J., and Wang, Y.: Characteristics and sources of
601 hourly trace elements in airborne fine particles in urban Beijing, China, *J. Geophys. Res. Atmos.*, 124,
602 11595-11613, <https://doi.org/10.1029/2019JD030881>, 2019.
- 603 [D'Alessandro, A., Lucarelli, F., Mandò, P.A., Marazzan, G., Nava, S., Prati, P., Valli, G., Vecchi, R.,
604 Zucchiatti, A.: Hourly elemental composition and sources identification of fine and coarse PM₁₀
605 particulate matter in four Italian towns, *J. Aerosol Sci.*, 34, 243-259, 2003.](https://doi.org/10.1016/j.jaerosci.2003.04.001)

606

607 Dall'esteOsto, M., Querol, X., Amato, F., Karanasiou, A., Lucarelli, F., Nava, S., Calzolari, G., and Chiari,
608 M.: Hourly elemental concentrations in PM_{2.5} aerosols sampled simultaneously at urban background
609 and road site during SAPUSS -diurnal variations and PMF receptor modelling, *Atmos. Chem. Phys.*,
610 13, 4375-4392, 2013.

611 Das, R., Mohtar, A.T.B.M., Rakshit, D., Shome, D., and Wang, X.: Sources of atmospheric lead (Pb) in
612 and around an Indian megacity, *Atmos. Environ.*, 193, 57-65,
613 <https://doi.org/10.1016/j.atmosenv.2018.08.062>, 2018.

614 Duan, J. and Tan, J.: Atmospheric heavy metals and arsenic in China: situation, sources and control
615 policies, *Atmos. Environ.*, 74, 93-101, 10.1016/j.atmosenv.2013.03.031, 2013.

616 Fang, B., Zhang, L., Zeng, H., Liu, J., Yang, Z., Wang, H., Wang, Q., and Wang, M.: PM_{2.5}-bound
617 polycyclic aromatic hydrocarbons: sources and health risk during non-heating and heating periods
618 (Tangshan, China), *Int. J. Env. Res. Pub. He.*, 17, 483, 2020.

619 Fernandez, J.A., Rey, A., and Carballeira, A.: An extended study of heavy metal deposition in Galicia
620 (NW Spain) based on moss analysis, *Sci. Total Environ.*, 254, 31-44, 10.1016/s0048-9697(00)00431-
621 9, 2000.

622 Furger, M., Minguillon, M.C., Yadav, V., Slowik, J.G., Hüglin, C., Fröhlich, R., Petterson, K.,
623 Baltensperger, U., and Prevot, A.S.H.: Elemental composition of ambient aerosols measured with high
624 temporal resolution using an online XRF spectrometer, *Atmos. Meas. Tech.*, 10, 2061-2076,
625 <https://doi.org/10.5194/amt-10-2061-2017>, 2017.

626 Geng, G., Xiao, Q., Zheng, Y., Tong, D., Zhang, Y., Zhang, X., Zhang, Q., He, K., and Liu, Y.: Impact of
627 China's air pollution prevention and control action plan on PM_{2.5} chemical composition over eastern
628 China, *Sci. China Earth Sci.*, 62, 1872-1884, <https://doi.org/10.1007/s11430-018-9353-x>, 2019.

629 [Grivas, G., Cheristanidis, S., Chaloulakou, A., Koutrakis, P., & Mihalopoulos, N.: Elemental composition
630 and source apportionment of fine and coarse particles at traffic and urban background locations in
631 Athens, Greece, *Aerosol Air Qual. Res.*, 18, 1642-1659, 2018.](#)

632 Guo, J., Tilgner, A., Yeung, C., Wang, Z., Louie, P.K.K., Luk, C.W.Y., Xu, Z., Yuan, C., Gao, Y., and
633 Poon, S.: Atmospheric peroxides in a polluted subtropical environment: seasonal variation, sources
634 and sinks, and importance of heterogeneous processes, *Environ. Sci. Technol.*, 48, 1443-1450,
635 <https://doi.org/10.1021/es403229x>, 2014.

636 Harmens, H., Norris, D.A., Steinnes, E., Kubin, E., Piispanen, J., Alber, R., Aleksiyenak, Y., Blum, O.,
637 Coskun, M., and Dam, M.: Mosses as biomonitors of atmospheric heavy metal deposition: Spatial
638 patterns and temporal trends in Europe, *Environ. Pollut.*, 158, 3144-3156,
639 <https://doi.org/10.1016/j.envpol.2010.06.039>, 2010.

640 He, Q., Zhang, M., Song, Y., and Huang, B.: Spatiotemporal assessment of PM_{2.5} concentrations and
641 exposure in China from 2013 to 2017 using satellite-derived data, *J. Cleaner Prod.*, 286, 124965,
642 <https://doi.org/10.1016/j.jclepro.2020.124965>, 2021.

643 Hjortenkrans, D.S., Bergbäck, B.G., and Häggerud, A.V.: Metal emissions from brake linings and tires:
644 case studies of Stockholm, Sweden 1995/1998 and 2005, *Environ. Sci. Technol.*, 41, 5224-5230,
645 <https://doi.org/10.1021/es070198o>, 2007.

646 Holden, P.A., Gardeatorresdey, J.L., Klaessig, F., Turco, R.F., Mortimer, M., Hundrinke, K., Hubal,
647 E.A.C., Avery, D., Barcelo, D., and Behra, R.: Considerations of environmentally relevant test
648 conditions for improved evaluation of ecological hazards of engineered nanomaterials, *Environ. Sci.*
649 *Technol.*, 50, 6124-6145, <https://doi.org/10.1021/acs.est.6b00608>, 2016.

650 Huang, C., Bao, L., Luo, P., Wang, Z., Li, S., and Zeng, E.Y.: Potential health risk for residents around a

651 typical e-waste recycling zone via inhalation of size-fractionated particle-bound heavy metals, *J.*
652 *Hazard. Mater.*, 317, 449-456, 10.1016/j.jhazmat.2016.05.081, 2016.

653 Jeong, C., Wang, J.M., and Evans, G.J.: Source apportionment of urban particulate matter using hourly
654 resolved trace metals, organics, and inorganic aerosol components, *Atmos. Chem. Phys.*, 1-32,
655 <https://doi.org/10.5194/acp-2016-189>, 2016.

656 Kamal, A., Cincinelli, A., Martellini, T., and Malik, R.N.: A review of PAH exposure from the combustion
657 of biomass fuel and their less surveyed effect on the blood parameters, *Environ. Sci. Pollut. Res.*, 22,
658 4076-4098, 10.1007/s11356-014-3748-0, 2015.

659 Kang, S., Chen, P., Li, C., Liu, B., and Cong, Z.: Atmospheric aerosol elements over the inland Tibetan
660 Plateau: concentration, seasonality, and transport, *Aerosol Air Qual. Res.*, 16, 789-800, 2016.

661 [Ke, H.B., Gong, S.L., He, J.J., Zhou, C.H., Zhang, L., Zhou, Y.K.: Spatial and temporal distribution of](#)
662 [open bio-mass burning in China from 2013 to 2017, *Atmos. Environ.*, 210, 156-165, 2019.](#)

663 Li, R., Fu, H., Cui, L., Li, J., Wu, Y., Meng, Y., Wang, Y., and Chen, J.: The spatiotemporal variation and
664 key factors of SO₂ in 336 cities across China, *J. Cleaner Prod.*, 210, 602-611,
665 <https://doi.org/10.1016/j.jclepro.2018.11.062>, 2019.

666 Li, R., Zhao, Y., Fu, H., Chen, J., Peng, M., and Wang, C.: Substantial changes in gaseous pollutants and
667 chemical compositions in fine particles in the North China Plain during the COVID-19 lockdown
668 period: anthropogenic vs. meteorological influences, *Atmos. Chem. Phys.*, 21, 8677-8692,
669 <https://doi.org/10.5194/acp-21-8677-2021>, 2021.

670 Li, R., Peng, M., Zhao, W.D., Wang, G.H., and Hao, J.M.: Data for “Measurement Report: Rapid changes
671 of chemical characteristics and health risks for high time-resolved trace elements in PM_{2.5} in a typical
672 industrial city in response to stringent clean air actions”, [dataset],
673 https://zenodo.org/record/7031975#_Ywys8cjfmfU, 2022.

674 Li, Z., Jiang, J., Ma, Z., Fajardo, O.A., Deng, J., and Duan, L.: Influence of flue gas desulfurization (FGD)
675 installations on emission characteristics of PM_{2.5} from coal-fired power plants equipped with selective
676 catalytic reduction (SCR), *Environ. Pollut.*, 230, 655-662,
677 <https://doi.org/10.1016/j.envpol.2017.06.103>, 2017.

678 Li, Z., Wang, Y., Li, Z., Guo, S., and Hu, Y.: Levels and sources of PM_{2.5}-associated pahs during and after
679 the wheat harvest in a central rural area of the beijing-tianjin-hebei (bth) region, *Aerosol Air Qual.*
680 *Res.*, 20, 1070-1082, 2020.

681 Lin, Y., Hsu, S., Chou, C.C.K., Zhang, R., Wu, Y., Kao, S., Luo, L., Huang, C., Lin, S., and Huang, Y.:
682 Wintertime haze deterioration in Beijing by industrial pollution deduced from trace metal fingerprints
683 and enhanced health risk by heavy metals, *Environ. Pollut.*, 208, 284-293,
684 <https://doi.org/10.1016/j.envpol.2015.07.044>, 2016.

685 Liu, H., He, K., Wang, Q., Huo, H., Lents, J., Davis, N., Nikkila, N., Chen, C., Osses, M., and He, C.:
686 Comparison of vehicle activity and emission inventory between Beijing and Shanghai, *J. Air Waste*
687 *Manage.*, 57, 1172-1177, <https://doi.org/10.3155/1047-3289.57.10.1172>, 2007.

688 Liu, J., Chen, Y., Chao, S., Cao, H., Zhang, A., and Yang, Y.: Emission control priority of PM_{2.5}-bound
689 heavy metals in different seasons: A comprehensive analysis from health risk perspective, *Sci. Total*
690 *Environ.*, 644, 20-30, <https://doi.org/10.1016/j.scitotenv.2018.06.226>, 2018a.

691 Liu, R., Men, C., Yu, W., Xu, F., Wang, Q., and Shen, Z.: Uncertainty in positive matrix factorization
692 solutions for PAHs in surface sediments of the Yangtze River Estuary in different seasons,
693 *Chemosphere*, 191, 922-936, <https://doi.org/10.1016/j.chemosphere.2017.10.070>, 2018b.

694 Lopez-Cruz, J., Crespo-Salvador, O., Fernandez-Crespo, E., Garcia-Agustin, P., and Gonzalez-Bosch, C.:

695 Absence of Cu-Zn-superoxide dismutase BCSOD1 reduces Botrytis cinerea virulence in Arabidopsis
696 and in tomato plants, which reveals interplay among ROS, callose and signaling pathways, Mol. Plant
697 Pathol., 18, 16-31, 2016.

698 [Lyu, X.P., Chen, N., Guo, H., Zeng, L.W., Zhang, W.H., Shen, F., Quan, J.H., Wang, N.: Chemical](#)
699 [characteristics and causes of airborne particulate pollution in warm seasons in Wuhan, central China,](#)
700 [Atmos. Chem. Phys., 16, 10671-10687, www.atmos-chem-phys.net/16/10671/2016/, 2016](#)

701 Lyu, Y., Zhang, K., Chai, F., Cheng, T., Yang, Q., Zheng, Z., and Li, X.: Atmospheric size-resolved trace
702 elements in a city affected by non-ferrous metal smelting: Indications of respiratory deposition and
703 health risk, Environ. Pollut., 224, 559-571, <https://doi.org/10.1016/j.envpol.2017.02.039>, 2017.

704 Ma, Z., Liu, R., Liu, Y., and Bi, J.: Effects of air pollution control policies on PM_{2.5} pollution
705 improvement in China from 2005 to 2017: a satellite-based perspective, Atmos. Chem. Phys., 19,
706 6861-6877, <https://doi.org/10.5194/acp-19-6861-2019>, 2019.

707 Manju, A., Kalaiselvi, K., Dhananjayan, V., Palanivel, M., Banupriya, G., Vidhya, M., Panjakumar, K.,
708 and Ravichandran, B.: Spatio-seasonal variation in ambient air pollutants and influence of
709 meteorological factors in Coimbatore, southern India, Air Qual. Atmos. Heal., 11, 1179-1189,
710 <https://doi.org/10.1007/s11869-018-0617-x>, 2018.

711 Manousakas, M., Papaefthymiou, H., Diapouli, E., Migliori, A., Karydas, A.G., Bogdanovic-
712 ~~radovic~~Radovic, I., and Eleftheriadis, K.: Assessment of PM_{2.5} sources and their corresponding level
713 of uncertainty in a coastal urban area using EPA PMF 5.0 enhanced diagnostics, Sci. Total Environ.,
714 574, 155-164, 2017.

715 Micheline, G., Rachida, C., Celine, M., Gaby, K., Rachid, A., and Petru, J.: Levels of Pb, Cd, Hg and As
716 in fishery products from the eastern Mediterranean and human health risk assessment due to their
717 Consumption, Interna. J. Environ. Res., 13, 443-455, <https://doi.org/10.1007/s41742-019-00185-w>,
718 2019.

719 Moreno, T., Querol, X., Alastuey, A., La Rosa, J.D.D., La Campa, A.M.S.D., Minguillon, M., Pandolfi,
720 M., Gonzalez-~~eastanedo~~Castanedo, Y., Monfort, E., and Gibbons, W.: Variations in vanadium, nickel
721 and lanthanoid element concentrations in urban air, Sci. Total Environ., 408, 4569-4579,
722 <https://doi.org/10.1016/j.scitotenv.2010.06.016>, 2010.

723 [Norris, G., Duvall, R., Brown, S., and Bai, S.: EPA positive matrix factorization \(PMF\) 5.0 fundamentals](#)
724 [and user guide. U.S. Environmental Protection Agency Office of Research and Development,](#)
725 [Washington, DC, 20460. \(i-124, EPA/600/R-14/108, April\), 2014.](#)

726 Oldani, K.M., Mladenov, N., Williams, M., Campbell, C.M., and Lipson, D.A.: Seasonal patterns of dry
727 deposition at a high-elevation site in the colorado rocky mountains, J. Geophys. Res. Atmos., 122,
728 11183-11200, 2017.

729 Olujimi, O.O., Oputu, O., Fatoki, O.S., Opatoyinbo, O.E., Aroyewun, O.A., and Baruani, J.: Heavy
730 metals speciation and human health risk assessment at an illegal gold mining site in Igun, Osun State,
731 Nigeria, J. Health. Pollut., 5, 19-32, 2015.

732 Paatero, P. and Tapper, U.: Positive matrix factorization: A non-negative factor model with optimal
733 utilization of error estimates of data values, Environmetrics, 5, 111-126, 1994.

734 Pacyna, J.M. and Pacyna, E.G.: An assessment of global and regional emissions of trace metals to the
735 atmosphere from anthropogenic sources worldwide, Environ. Rev., 9, 269-298, 2001.

736 [Prati, P., Zucchiatti, A., Lucarelli, F., Mandò, P.A.: Source apportionment near a steel plant in Genoa](#)
737 [\(Italy\) by continuous aerosol sampling and PIXE analysis, Atmos. Environ., 34, 3149-3157, 2000.](#)

738 Rai, P.K., Lee, S.S., Zhang, M., Tsang, Y.F., and Kim, K.: Heavy metals in food crops: Health risks, fate,

739 mechanisms, and management, *Environ. Interna.*, 125, 365-385, 2019.

740 Rasmussen, P.E.: Long-range atmospheric transport of trace metals: the need for geoscience perspectives,
741 *Environ. Earth Sci.*, 33, 96-108, 1998.

742 Reff, A., Eberly, S.I., and Bhave, P.V.: Receptor modeling of ambient particulate matter data using
743 positive matrix factorization: review of existing methods, *J. Air Waste Manage.*, 57, 146-154, 2007.

744 Ren, Z., Zhang, B., Lu, P., Li, C., Gao, L., and Zheng, M.: Characteristics of air pollution by
745 polychlorinated dibenzo-p-dioxins and dibenzofurans in the typical industrial areas of Tangshan City,
746 China, *J. Environ. Sci. -China*, 23, 228-235, 2011.

747 Saffari, A., Daher, N., Shafer, M.M., Schauer, J.J., and Sioutas, C.: ~~global~~Global perspective on the
748 oxidative potential of airborne particulate matter: a synthesis of research findings, *Environ. Sci.*
749 *Technol.*, 48, 7576-7583, 2014.

750 Shafer, M.M., Toner, B.M., Overdier, J.T., Schauer, J.J., Fakra, S.C., Hu, S., Herner, J.D., and Ayala, A.:
751 Chemical speciation of vanadium in particulate matter emitted from diesel vehicles and urban
752 atmospheric aerosols, *Environ. Sci. Technol.*, 46, 189-195, 2012.

753 Shi, G., Teng, J., Ma, H., Li, Y., and Sun, B.: Metals and metalloids in precipitation collected during
754 CHINARE campaign from Shanghai, China, to Zhongshan Station, Antarctica: Spatial variability and
755 source identification, *Global Biogeochem. Cyc.*, 29, 760-774, 2015.

756 Song, Z.F.: An assessment of the heavy metal pollution and potential ecological hazards in urban soil of
757 Tangshan City, *Geology in China* 38, 1379-1386, 2011.

758 Storelli, M.M.: Potential human health risks from metals (Hg, Cd, and Pb) and polychlorinated biphenyls
759 (PCBs) via seafood consumption : estimation of target hazard quotients (THQs) and toxic equivalents
760 (TEQs), *Food and Chemical Toxicology* 46, 2782-2788, 2008.

761 Taghvaei, S., Sowlat, M.H., Mousavi, A., Hassanvand, M.S., Yunesian, M., Naddafi, K., and Sioutas, C.:
762 Source apportionment of ambient PM_{2.5} in two locations in central Tehran using the Positive Matrix
763 Factorization (PMF) model, *Sci. Total Environ.*, 628-629, 672-686, 2018.

764 Tang, Q., Sheng, W., Li, L., Zheng, L., Miao, C., and Sun, R.: Alteration behavior of mineral structure
765 and hazardous elements during combustion of coal from a power plant at Huainan, Anhui, China,
766 *Environ. Pollut.*, 239, 768-776, 2018.

767 Tian, H., Zhu, C., Gao, J., Cheng, K., Hao, J., Wang, K., Hua, S., Wang, Y., and Zhou, J.: Quantitative
768 assessment of atmospheric emissions of toxic heavy metals from anthropogenic sources in China:
769 historical trend, spatial distribution, uncertainties, and control policies, *Atmos. Chem. Phys.*, 15,
770 10127-10147, 2015.

771 Tianxue, W., Yuesi, W., Shihyu, C., and Guangren, L.: On-line measurement of water-soluble ions in
772 ambient particles, *Adv. Atmos. Sci.*, 23, 586-592, 2006.

773 Wang, S., Su, H., Chen, C., Tao, W., Streets, D.G., Lu, Z., Zheng, B., Carmichael, G.R., Lelieveld, J.,
774 and Pöschl, U.: Natural gas shortages during the “coal-to-gas” transition in China have caused a large
775 redistribution of air pollution in winter 2017, *P. Natl. Acad. Sci. USA*, 117, 31018-31025, 2020a.

776 Wang, S., Su, H., Chen, C., Tao, W., Streets, D.G., Lu, Z., Zheng, B., Carmichael, G.R., Lelieveld, J.,
777 Pöschl, U., and Cheng, Y.: Natural gas shortages during the “coal-to-gas” transition in China have
778 caused a large redistribution of air pollution in winter 2017, *P. Natl. Acad. Sci. USA*, 117, 31018-
779 31025, 2020b.

780 Westerdahl, D., Wang, X., Pan, X., and Zhang, K.M.: Characterization of on-road vehicle emission
781 factors and microenvironmental air quality in Beijing, China, *Atmos. Environ.*, 43, 697-705,
782 <https://doi.org/10.1016/j.atmosenv.2008.09.042>, 2009.

783 Witt, M.L.I., Baker, A.R., and Jickells, T.D.: Atmospheric trace metals over the Atlantic and South Indian
784 Oceans: Investigation of metal concentrations and lead isotope ratios in coastal and remote marine
785 aerosols, *Atmos. Environ.*, 40, 5435-5451, <https://doi.org/10.1016/j.atmosenv.2006.04.041>, 2006.

786 Wu, Q., Wang, S., Zhang, L., Song, J., Yang, H., and Meng, Y.: Update of mercury emissions from China's
787 primary zinc, lead and copper smelters, 2000-2010, *Atmos. Chem. Phys.*, 12, 18207-18242,
788 <https://doi.org/10.5194/acp-12-11153-2012>, 2012.

789 Wu, Y., Wang, R., Zhou, Y., Lin, B., Fu, L., He, K., and Hao, J.: ~~en~~On-road vehicle emission control in
790 beijing: past, present, and future, *Environ. Sci. Technol.*, 45, 147-153,
791 <https://doi.org/10.1021/es1014289>, 2011.

792 Xiao, Q., Geng, G., Liang, F., Wang, X., Lv, Z., Lei, Y., Huang, X., Zhang, Q., Liu, Y., and He, K.:
793 Changes in spatial patterns of PM_{2.5} pollution in China 2000-2018: Impact of clean air policies,
794 *Environ. Internat.*, 141, 105776, <https://doi.org/10.1016/j.envint.2020.105776>, 2020.

795 Yang, Q., Yuan, Q., Li, T., Shen, H., and Zhang, L.: The relationships between PM_{2.5} and meteorological
796 factors in China: seasonal and regional variations, *Int. J. Env. Res. Pub. He.*, 14, 1510, 2017.

797 Yi, Y., Yang, Z., and Zhang, S.: Ecological risk assessment of heavy metals in sediment and human health
798 risk assessment of heavy metals in fishes in the middle and lower reaches of the Yangtze River basin,
799 *Environ. Pollut.*, 159, 2575-2585, <https://doi.org/10.1016/j.envpol.2011.06.011>, 2011.

800 Yu, L., Wang, G., Zhang, R., Zhang, L., Song, Y., Wu, B., Li, X., An, K., and Chu, J.: ~~eharacterization~~
801 Characterization and source apportionment of pm_{2.5} in an urban environment in Beijing, *Aerosol Air*
802 *Qual. Res.*, 13, 574-583, doi: 10.4209/aaqr.2012.07.0192, 2013.

803 Zhang, J., Zhou, X., Wang, Z., Yang, L., Wang, J., Wang, W.: Trace elements in PM_{2.5} in Shandong
804 Province: Source identification and health risk assessment, *Sci. Total Environ.*, 621, 558-577, 2018.

805 Zhang, Q., Zheng, Y., Tong, D., Shao, M., Wang, S., Zhang, Y., Xu, X., Wang, J., He, H., Liu, W., Ding,
806 Y., Lei, Y., Li, J., Wang, Z., Zhang, X., Wang, Y., Cheng, J., Liu, Y., Shi, Q., Yan, L., Geng, G., Hong,
807 C., Li, M., Liu, F., Zheng, B., Cao, J., Ding, A., Gao, J., Fu, Q., Huo, J., Liu, B., Liu, Z., Yang, F., He,
808 K., and Hao, J.: Drivers of improved PM_{2.5} air quality in China from 2013 to 2017, *P. Natl. Acad. Sci.*
809 *USA*, 116, 24463-24469, <https://doi.org/10.1073/pnas.1907956116>, 2019.

810 Zhao, M., Zhang, Y., Ma, W., Fu, Q., Yang, X., Li, C., Zhou, B., Yu, Q., and Chen, L.: Characteristics
811 and ship traffic source identification of air pollutants in China's largest port, *Atmos. Environ.*, 64, 277-
812 286, <https://doi.org/10.1016/j.atmosenv.2012.10.007>, 2013.

813 Zhu, C., Tian, H., Hao, Y., Gao, J., Hao, J., Wang, Y., Hua, S., Wang, K., and Liu, H.: A high-resolution
814 emission inventory of anthropogenic trace elements in Beijing-Tianjin-Hebei (BTH) region of China,
815 *Atmos. Environ.*, 191, 452-462, <https://doi.org/10.1016/j.atmosenv.2018.08.035>, 2018.

816 Zhu, C., Tian, H., and Hao, J.: Global anthropogenic atmospheric emission inventory of twelve typical
817 hazardous trace elements, 1995-2012, *Atmos. Environ.*, 220, 117061,
818 <https://doi.org/10.1016/j.atmosenv.2019.117061>, 2020.

819

设置了格式: 下标

Figure 1 Topographic map of China indicating the location of Tangshan (a), the sampling site (b), and some major industrial points (b). The population distribution of Tangshan is also depicted in (b).

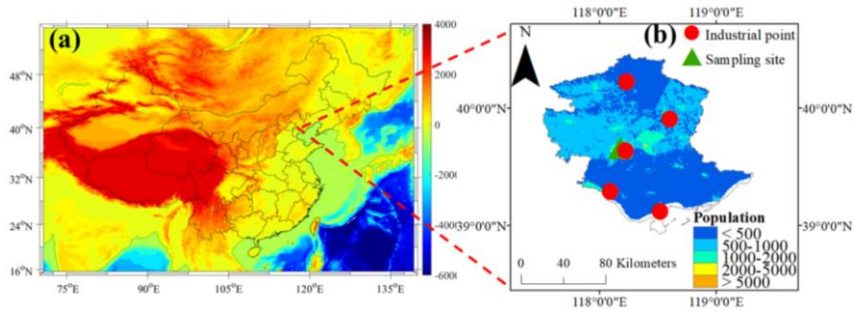


Figure 2 Bar chart of the concentrations of 16 trace elements including K, Fe, Ca, Zn, Pb, Mn, Fe, As, Se, V, Cr, Ag, Ni, Hg, Ga, and Co. The bar and black line represent mean values and associated standard deviations, respectively.

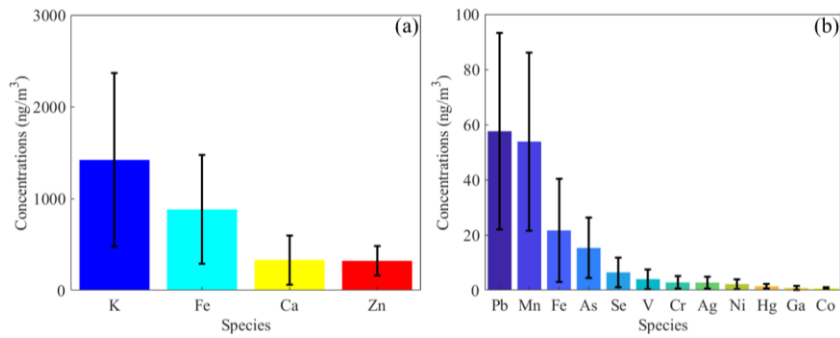


Figure 3 Inter-annual variations of the original (red) and deweathered (manganese purple) element concentrations (ng/m^3) in $\text{PM}_{2.5}$ in Tangshan. The dark, nattier blue, and nattier yellow backgrounds represent the species during 2017-2018 (from September in 2017 to August in 2018), 2018-2019 (from September in 2018 to August in 2019), and 2019-2020 (from September in 2019 to August in 2020). The bar and black line represent mean values and associated standard deviations, respectively.

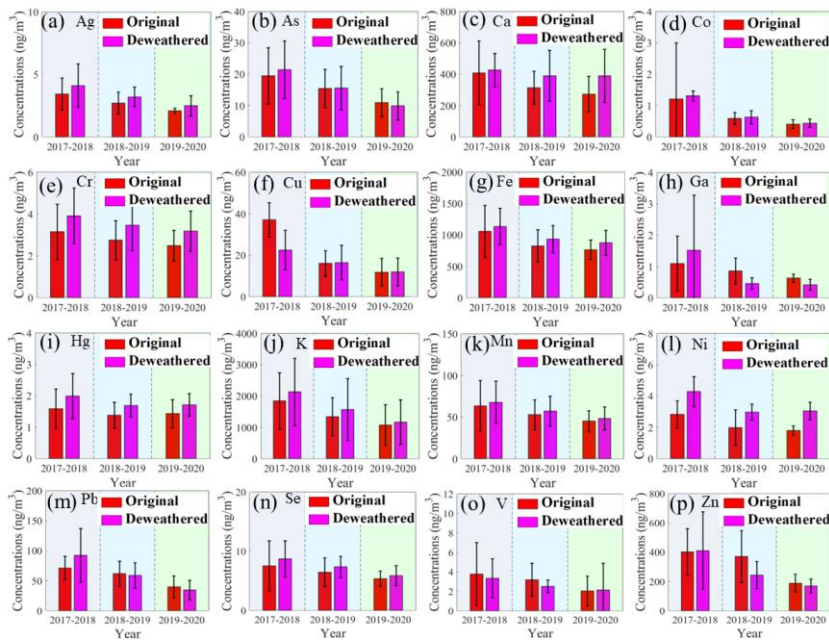


Figure 4 Original (red and orange) and deweathered (green and blue) element concentrations (ng/m^3) in $\text{PM}_{2.5}$ in Tangshan in four seasons during 2017-2018, 2018-2019, and 2019-2020. S1, U1, A1, and W1 represent the spring, summer, autumn, and winter during 2017-2018. S2, U2, A2, and W2 denote the spring, summer, autumn, and winter during 2018-2019. S3, U3, A3, and W3 are the spring, summer, autumn, and winter during 2019-2020. The point and shaded area represent mean values and associated standard deviations, respectively.

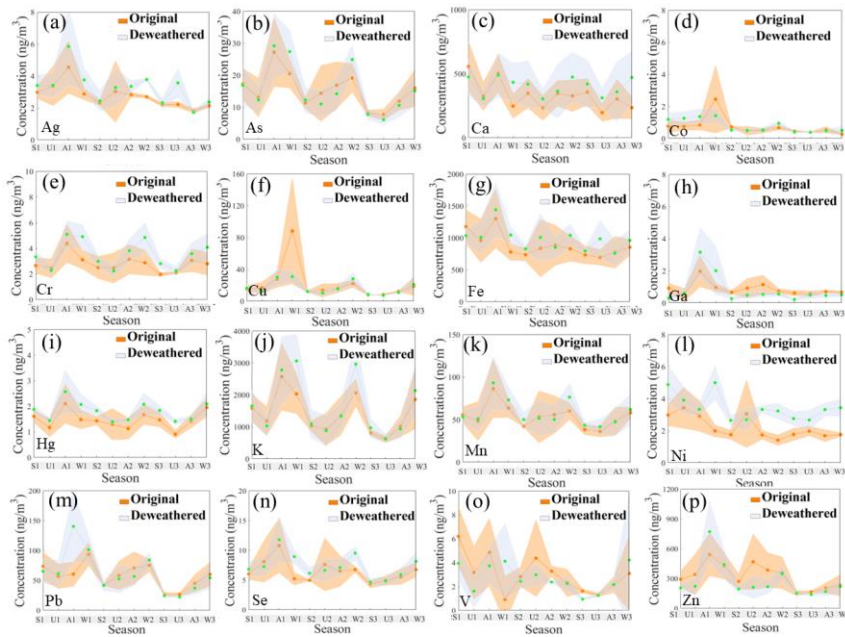


Figure 5 Weekly variations of original (green) and deweathered (orange) element concentrations (ng/m^3) in $\text{PM}_{2.5}$ in Tangshan. The green and dark backgrounds denote the error bars of original and deweathered elements, respectively. The bar and black line represent mean values and associated standard deviations, respectively.

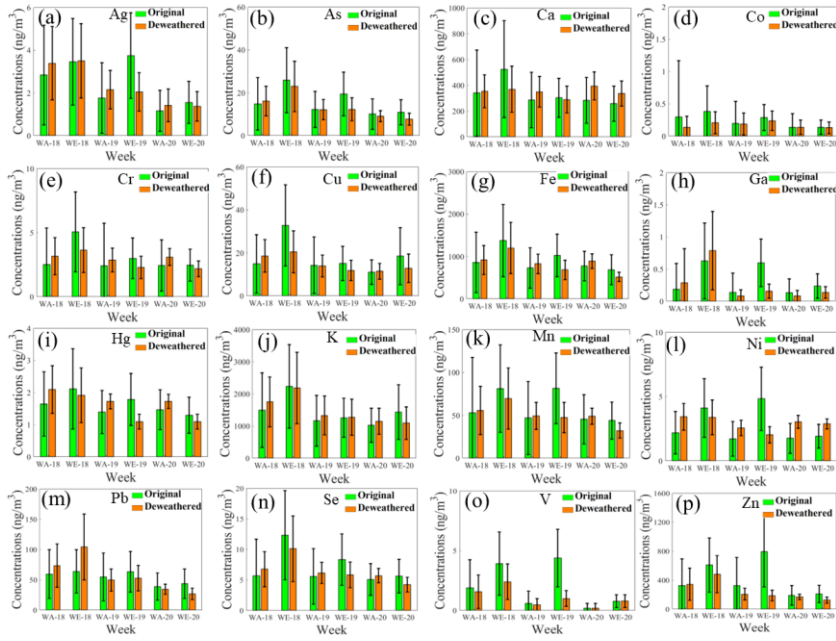


Figure 6 Relative importance of the predictors for the prediction of trace elements. The columns in the figure represent the variable importance in the RF models for the trace elements. P, RH, T, WD, WS, DOW, HOY, DOY, and Year denote air pressure, relative humidity, air temperature, wind direction, wind speed, day of week, hour of day, day of year, and study year, respectively.

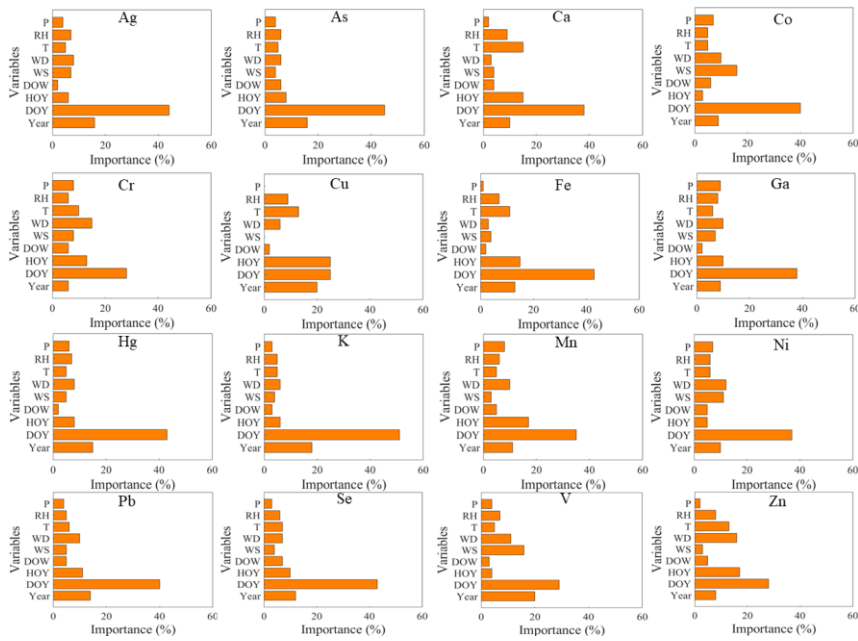


Figure 7 Deweathered concentrations of trace elements derived from six sources in Tangshan during 2017-2020.

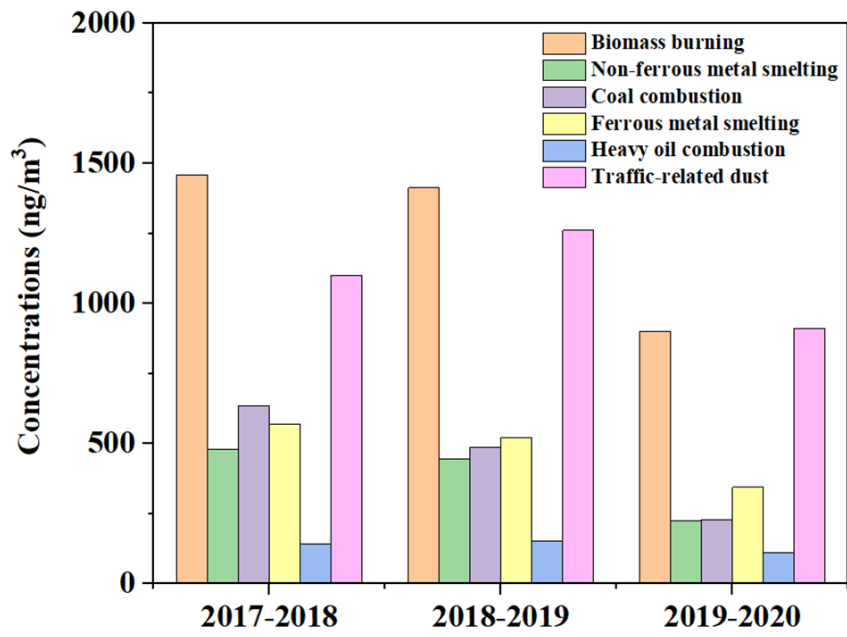


Figure 8 Average contributions of the six sources to the deweathered concentrations of elements in PM_{2.5} based on the PMF model. The red panel means the biomass burning; the green panel denotes the non-ferrous metal smelting; the blue one represents the coal combustion; the cyan one is the ferrous metal smelting; the pink one represents the heavy oil combustion; and the yellow one denotes the traffic-related dust. (a), (b), and (c) represent the source contributions during 2017-2018, 2018-2019, and 2019-2020, respectively.

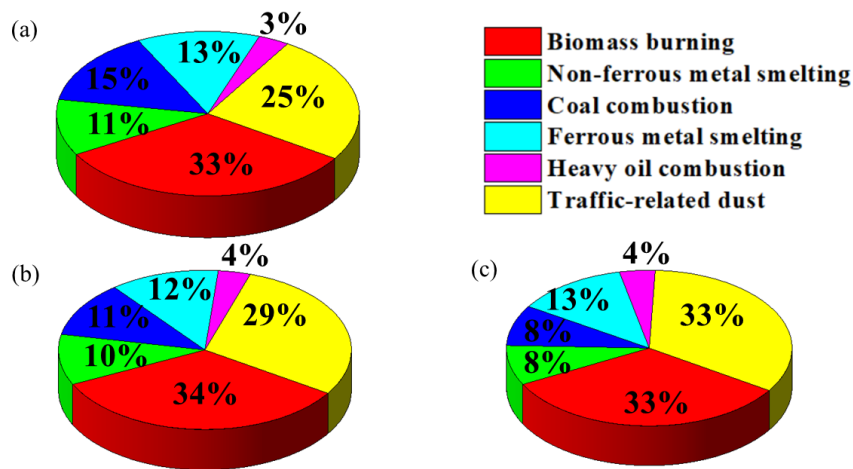


Table 1 Comparison of the element concentrations in PM_{2.5} of Tangshan and the standard values for these elements in World Health Organization (WHO), China, Europe, and the United States (Unit: ng/m³).

| Elements | Mean±SD | CAAQS | WHO | EU | United States |
|----------|-----------|-------|------|----|---------------|
| Co | 0.74±0.24 | | | | |
| Ga | 0.86±0.74 | | | | |
| Hg | 1.47±0.81 | 50 | 1000 | | |
| Ni | 2.21±1.80 | | 25 | 20 | |
| Ag | 2.75±2.08 | | | | |
| Cr | 2.80±2.22 | 0.025 | 0.25 | | |
| V | 3.98±3.57 | | | | |
| Se | 6.46±5.28 | | | | |
| As | 15.3±11.0 | 6 | 6.60 | 6 | |
| Cu | 21.7±18.7 | | | | |
| Mn | 53.8±32.3 | | | | |
| Pb | 57.6±35.7 | | 1000 | | 150 |
| Zn | 320±162 | | | | |
| Ca | 332±268 | | | | |
| Fe | 881 ± 591 | | | | |
| K | 1421±947 | | | | |

Table 2 Non-carcinogenic and carcinogenic risks for the original element levels in PM_{2.5}.

| Age | Year | Indicator | Cr | Mn | Fe | Co | Ni | Cu | Zn | As | Pb |
|-----------|-----------|-----------------------|-----------------------|-----------------------|-----------------------|-----------------------|-----------------------|-----------------------|-----------------------|------------------|------------------|
| Adult | 2017-2018 | HQ | 2.47×10 ⁻⁴ | 1.07×10 ⁻⁴ | 3.55×10 ⁻⁴ | 4.50×10 ⁻⁴ | 0.33×10 ⁻⁴ | 1.18×10 ⁻⁴ | 3.15×10 ⁻⁴ | 1.53× | 8.39× |
| | | | | | | | | | | 10 ⁻² | 10 ⁻³ |
| | | CR | 0.13×10 ⁻⁶ | -- | -- | -- | -- | -- | -- | 2.37× | 2.88× |
| | | | | | | | | | | 10 ⁻⁶ | 10 ⁻⁶ |
| | 2018-2019 | HQ | 2.16×10 ⁻⁴ | 0.89×10 ⁻⁴ | 2.77×10 ⁻⁴ | 4.67×10 ⁻⁴ | 0.23×10 ⁻⁴ | 0.95×10 ⁻⁴ | 2.91×10 ⁻⁴ | 1.21× | 7.28× |
| | | | | | | | | | | 10 ⁻² | 10 ⁻³ |
| | CR | 0.11×10 ⁻⁶ | -- | -- | -- | -- | -- | -- | 1.87× | 2.50× | |
| | | | | | | | | | 10 ⁻⁶ | 10 ⁻⁶ | |
| 2019-2020 | HQ | 1.95×10 ⁻⁴ | 0.76×10 ⁻⁴ | 2.58×10 ⁻⁴ | 3.26×10 ⁻⁴ | 0.21×10 ⁻⁴ | 0.70×10 ⁻⁴ | 1.49×10 ⁻⁴ | 0.86× | 4.69× | |
| | | | | | | | | | 10 ⁻² | 10 ⁻³ | |
| | CR | 0.10×10 ⁻⁶ | -- | -- | -- | -- | -- | -- | 1.33× | 1.61× | |
| | | | | | | | | | 10 ⁻⁶ | 10 ⁻⁶ | |
| Child | 2017-2018 | HQ | 6.02×10 ⁻⁴ | 2.60×10 ⁻⁴ | 8.64×10 ⁻⁴ | 11.1×10 ⁻⁴ | 0.81×10 ⁻⁴ | 2.87×10 ⁻⁴ | 7.67×10 ⁻⁴ | 3.73× | 20.4× |
| | | | | | | | | | | 10 ⁻² | 10 ⁻³ |
| | | CR | 0.08×10 ⁻⁶ | -- | -- | -- | -- | -- | -- | 1.44× | 1.75× |
| | | | | | | | | | | 10 ⁻⁶ | 10 ⁻⁶ |
| | 2018-2019 | HQ | 5.26×10 ⁻⁴ | 2.17×10 ⁻⁴ | 6.74×10 ⁻⁴ | 11.0×10 ⁻⁴ | 0.57×10 ⁻⁴ | 2.30×10 ⁻⁴ | 7.08×10 ⁻⁴ | 2.95× | 17.7× |
| | | | | | | | | | | 10 ⁻² | 10 ⁻³ |
| | CR | 0.07×10 ⁻⁶ | -- | -- | -- | -- | -- | -- | 1.14× | 1.52× | |
| | | | | | | | | | 10 ⁻⁶ | 10 ⁻⁶ | |

| | | | | | | | | | | |
|-----------|----|--------------------|--------------------|--------------------|--------------------|--------------------|--------------------|--------------------|--------|--------|
| 2019-2020 | HQ | 4.75×10^4 | 1.85×10^4 | 6.27×10^4 | 7.93×10^4 | 0.52×10^4 | 1.70×10^4 | 3.61×10^4 | 2.09× | 11.4× |
| | | | | | | | | | 10^2 | 10^4 |
| | CR | 0.06×10^6 | -- | -- | -- | -- | -- | -- | 0.81× | 0.98× |
| | | | | | | | | | 10^6 | 10^6 |

Table 3 Non-carcinogenic and carcinogenic risks for the deweathered element levels in PM_{2.5}.

| Age | Year | Indicator | Cr | Mn | Fe | Co | Ni | Cu | Zn | As | Pb |
|-----------|-----------|-----------------------|-----------------------|-----------------------|-----------------------|-----------------------|-----------------------|-----------------------|-----------------------|-----------------|-----------------|
| Adult | 2017-2018 | HQ | 3.07×10^{-4} | 1.14×10^{-4} | 3.82×10^{-4} | 10.3×10^{-4} | 0.50×10^{-4} | 1.33×10^{-4} | 3.15×10^{-4} | 1.68× | 10.8× |
| | | | | | | | | | | 10 ² | 10 ³ |
| | | CR | 0.16×10^{-6} | -- | -- | -- | -- | -- | -- | 2.60× | 3.72× |
| | | | | | | | | | | 10 ⁶ | 10 ⁶ |
| | 2018-2019 | HQ | 2.73×10^{-4} | 0.96×10^{-4} | 3.14×10^{-4} | 4.93×10^{-4} | 0.35×10^{-4} | 0.97×10^{-4} | 2.91×10^{-4} | 1.22× | 6.91× |
| | | | | | | | | | | 10 ² | 10 ³ |
| | CR | 0.14×10^{-6} | -- | -- | -- | -- | -- | -- | 1.89× | 2.37× | |
| | | | | | | | | | 10 ⁶ | 10 ⁶ | |
| 2019-2020 | HQ | 2.50×10^{-4} | 0.82×10^{-4} | 2.95×10^{-4} | 3.46×10^{-4} | 0.36×10^{-4} | 0.70×10^{-4} | 1.49×10^{-4} | 0.78× | 4.08× | |
| | | | | | | | | | 10 ² | 10 ³ | |
| | CR | 0.13×10^{-6} | -- | -- | -- | -- | -- | -- | 1.20× | 1.40× | |
| | | | | | | | | | 10 ⁶ | 10 ⁶ | |
| Child | 2017-2018 | HQ | 7.47×10^{-4} | 2.77×10^{-4} | 9.28×10^{-4} | 11.7×10^{-4} | 1.23×10^{-4} | 3.22×10^{-4} | 3.23×10^{-4} | 4.09× | 26.4× |
| | | | | | | | | | | 10 ² | 10 ³ |
| | | CR | 0.10×10^{-6} | -- | -- | -- | -- | -- | -- | 1.58× | 2.26× |
| | | | | | | | | | | 10 ⁶ | 10 ⁶ |
| | 2018-2019 | HQ | 6.64×10^{-4} | 2.34×10^{-4} | 7.64×10^{-4} | 11.9×10^{-4} | 0.85×10^{-4} | 2.36×10^{-4} | 1.91×10^{-4} | 2.98× | 16.8× |
| | | | | | | | | | | 10 ² | 10 ³ |
| | CR | 0.09×10^{-6} | -- | -- | -- | -- | -- | -- | 1.15× | 1.44× | |
| | | | | | | | | | 10 ⁶ | 10 ⁶ | |

| | | | | | | | | | | |
|-----------|----|--------------------|--------------------|--------------------|--------------------|--------------------|--------------------|--------------------|--------|--------|
| 2019-2020 | HQ | 6.08×10^4 | 1.99×10^4 | 7.17×10^4 | 8.42×10^4 | 0.87×10^4 | 1.71×10^4 | 1.34×10^4 | 1.89× | 9.92× |
| | | | | | | | | | 10^2 | 10^4 |
| | CR | 0.08×10^6 | -- | -- | -- | -- | -- | -- | 0.73× | 0.85× |
| | | | | | | | | | 10^6 | 10^6 |
